Mechanical Systems and Signal Processing 66-67 (2016) 505–520

Contents lists available at ScienceDirect

Mechanical Systems and Signal Processing

journal homepage: www.elsevier.com/locate/ymssp

Multi-sensor data fusion framework for CNC machining monitoring

João A. Duro [a,*], Julian A. Padget [a], Chris R. Bowen [b], H. Alicia Kim [b], Aydin Nassehi [b]

[a] Department of Computer Science, University of Bath, Claverton Down BA2 7AY, UK
[b] Department of Mechanical Engineering, University of Bath, Claverton Down BA2 7AY, UK

ARTICLE INFO

Article history:
Received 25 June 2014
Received in revised form
23 March 2015
Accepted 16 April 2015
Available online 2 July 2015

Keywords:
CNC machining
Acoustic emission
Process monitoring
Multi-sensor data fusion

ABSTRACT

Reliable machining monitoring systems are essential for lowering production time and manufacturing costs. Existing expensive monitoring systems focus on prevention/detection of tool malfunctions and provide information for process optimisation by force measurement. An alternative and cost-effective approach is monitoring acoustic emissions (AEs) from machining operations by acting as a robust proxy. The limitations of AEs include high sensitivity to sensor position and cutting parameters. In this paper, a novel multi-sensor data fusion framework is proposed to enable identification of the best sensor locations for monitoring cutting operations, identifying sensors that provide the best signal, and derivation of signals with an enhanced periodic component. Our experimental results reveal that by utilising the framework, and using only three sensors, signal interpretation improves substantially and the monitoring system reliability is enhanced for a wide range of machining parameters. The framework provides a route to overcoming the major limitations of AE based monitoring.

1. Introduction

In the manufacturing sector there is an ever growing-demand to increase the quality and diversity of products, as well as lowering production time and costs. This is mostly due to intensified global competition, diversified demand and shrinkage of product life cycles [1,2]. To meet the above demands, manufacturers' interests are turning increasingly towards automated machining systems, where there is less dependence on the operator during the production process. The success of an automated machining system depends vastly on a robust and reliable monitoring system for on-line and off-line supervision of key machining processes. This is considered a challenging task due to the following main reasons [3]:

1. The geometrical complexity of the components that form the final machined product requires complex tool path strategies along with a variety of machining techniques, as found, for instance, in high-speed milling [4,5] and machining of sculptured surfaces [6].

* Corresponding author.
E-mail addresses: joao.duro@gmail.com (J.A. Duro), jap@bath.ac.uk (J.A. Padget), c.r.bowen@bath.ac.uk (C.R. Bowen), h.a.kim@bath.ac.uk (H.A. Kim), a.nassehi@bath.ac.uk (A. Nassehi).

http://dx.doi.org/10.1016/j.ymssp.2015.04.019
0888-3270/

2. Materials that possess low machinability such as difficult-to-cut nickel based and titanium superalloys can lead to tool failure during machining operations since they require more energy than that of lower strength materials. Some typical wear features that are caused during machining include rapid flank wear and notching [7].
3. Sensory signals derived from machining operations that could indicate the presence of machine failure are not always easy to interpret owing to the complexity of the cutting tool, and also due to its geometry and paths.
4. The high-cost associated with certain machining components which prevent the occurrence of wastage and/or any additional machining.

The application of intelligent systems to monitor computer numerical control (CNC) machining operations is rapidly increasing in the industry. Several approaches have been proposed that accomplish tool monitoring and some of them have been successfully adapted to industrial applications. An extensive review on sensor-based systems for tool condition monitoring with a special focus on industrial applications can be found in [8]. Despite earlier efforts, and due to the reasons mentioned above, the existing intelligent monitoring systems are still not considered reliable enough to completely replace human supervision. In that, human operators are still essential in the industry to detect the end of tool life and to correct the cutting parameters whenever it is required [9]. Currently, there are three main goals related to machining process monitoring:

(i) Prevent and detect any machining tool and workpiece malfunctions. This can reduce the number of scrapped components during machining operations and prevent any irreversible damage to the tool and/or final machined product.
(ii) Provision of information that can be utilised towards the machining process optimisation. For instance, in [10] energy consumption readings are utilised to optimise the process planning in CNC machining.
(iii) Contribution to the development of a database towards the determination of an optimal set of cutting (control) parameters for the given machining process.

An approach that is becoming increasingly popular is to analyse the acoustic emissions (AEs) derived from machining cutting operations. Despite their advantages, AE-based systems are not considered to be totally reliable due to (a) their sensitivity to AE generated by sources other than tool and workpiece which can be picked up by the sensor and confuse the signal processing task [11], (b) the requirements of adjusting the signal amplification which is dependent on the process to be monitored [12], (c) the sensitivity of the AE measurements to sensor location and cutting parameters [2], and (d) limitations related to the practical implementation of a microphone in an industrial setting, such as directional consideration, frequency response, and environmental sensitivity [13]. To address the above limitations, this paper proposes a multi-sensor data fusion framework that relies on the information captured by more than one sensor and subsequent processing allows for

1. Identification of which sensor provides the best signal representation and best location for monitoring the cutting operation. The identified sensor yields the highest periodic component strength that corresponds to the cutting tool rotation period.
2. Derivation of a signal with an enhanced periodic component corresponding to the cutting tool rotation period when compared with individual sensor signals. The derived signal, known as signal estimate, improves the signal representation by further enhancing the signal over the noise that best describes the cutting operation for the given cutting parameters.

To validate the proposed framework a set of three microphones are placed at different locations inside a CNC machining structure and measurements are taken for a wide range of cutting parameters.

The remaining structure of the paper is as follows: an introduction to acoustic emissions with special focus on machining applications is provided in Section 2, two approaches that form the basis for the proposed framework are described in Section 3 while Section 4 presents the framework. The experimental results on CNC machining data are covered in Section 5 and the paper concludes with Section 6.

2. Acoustic emissions monitoring in machining

The acoustic emissions (AEs), also known as “stress wave emission” or “microseismic activity”, are a phenomenon of sound and ultrasound wave radiation where elastic energy is released in the form of mechanical vibration from a material (tool, workpiece, machine body) as it undergoes deformation and fracture processes [11]. AE signals derived from machining operations (metal cutting in this instance) can be either (i) a transient signal, also called “burst”, characterised by a short duration signal with high-amplitude and associated with chip and tool fracture; or (ii) a continuous signal characterised by a long duration signal with variations in the amplitude and frequency, often associated with unwanted (noise) signals such as friction, deformation and flow noise [14,15]. The spectrum of a typical AE spans the kilohertz (kHz) to megahertz (MHz) range which is well above the machining operation frequency, characterised by the spindle rotation and the frequencies of the normal modes of operation. This has allowed the application of AE sensors for machining process monitoring that includes characterising the tool/workpiece surface/subsurface (roughness and anomalies), tool condition (e.g. tool wear and

tool breakage), and dimensional accuracy (bore size tolerance). A selection of applications currently found in the literature is summarised as follows:

1. *AE as a single sensor*: tool breakage [16], tool wear [17–19], tool wear and chipping [20], tool and workpiece malfunctions [3,21], and tool wear and surface roughness [22,23].
2. *AE together and/or combined with other sensors*: tool wear [24–29], tool breakage detection [30,31], surface roughness prediction [32], and dimensionality accuracy and surface roughness [33].

An acoustic emission wave travels omni-directionally from the source material to the AE sensor via the material itself and/or by air. This means that the AE sensors can be either attached or separated from the material. A direct measurement of the cutting process is possible if the sensor is either placed close or attached to the tool or workpiece. However, it is often the case that in the proximity of the cutting operation there is a substantial amount of material being removed and coolant fluid being delivered which makes it difficult, if not impossible, to conduct a direct measurement. On the other hand, although the remote placement provides more security to the capturing process itself, it might result in filtering and distortion of the signal. This can be attributed to the structures and substances that exists in the path of the cutting process and the sensor location [13].

The AE sensors have been categorised in [11] as either piezoelectric or dynamic microphones, and the two main differences are

(i) *The frequency range*: Where the typical piezoelectric AE sensor ranges from 10 kHz to 10 MHz while the microphones ranges from a few Hertz to a hundred kHz.
(ii) *The sensor placement*: Where the piezoelectric AE sensors are usually attached to the material to be monitored (often the tool or workpiece) while the microphones are placed away from the cutting operation.

Although most AE sensor applications in machining belong to the piezoelectric category [34], microphones have been utilised in the past for chatter detection in milling operations [13], for acoustic sensing in laser drilling [35], and more recently for CNC machining in woodworking operations [36] and for monitoring a gas metal arc welding process [37]. In [13] a comparison was made between a microphone and other remotely placed sensors, such as force dynamometers and accelerometers, and it is shown that the microphone provides the best balance in satisfying the many requirements of a sensor for the purpose of chatter detection and control in milling operations.

Another important aspect is the superior sensitivity and higher signal-to-noise ratio (SNR) of AE sensors for monitoring the most critical processes in precision machining when compared with other conventional types of sensors, such as force and vibration [38,39]. Conventional sensors suffer from inaccuracies due to loss of sensitivity in the extremely high frequency range, while AE sensors exhibit improved response in the high-frequency range where frequencies from submicrometre-level precision machining activity are more prominent. The sensors sensitivity is affected by the level of precision required by the machining process and as well by the control parameters to be monitored, as represented in Fig. 1. Notably, AE sensors are the most reliable sensors in dealing with surface roughness and subsurface damage when the level of precision increases to ultra-precision scale (1 nm). This means that AE sensors are suitable for monitoring micro-cutting mechanisms since noise from disturbance sources (bearings, slides, etc.) can be minimised.

3. Background theory

This section presents two approaches that form the basis of this paper's framework, namely maximum likelihood estimation and auto-correlation coefficient. The former provides a signal estimate based on the signal variance, under the assumption that a reasonable model for the noise is white Gaussian noise (WGN). The latter provides a measure of the periodic component strength that corresponds to the cutting tool rotation period, given that AE signals derived from rotary cutters are periodic by nature. The maximum likelihood estimation and the auto-correlation coefficient are detailed in Sections 3.1 and 3.2, respectively.

3.1. Maximum likelihood estimation

Maximum likelihood estimation (MLE) [40] is a standard approach for estimating the parameters of a given statistical model which is widely used due to its simplicity and often because it yields the most natural estimates [41].

Consider an ensemble of M observations of a noise-corrupted discrete-time N-point signal as

$$\mathbf{x}[n] = \begin{bmatrix} x_1[n] \\ x_2[n] \\ \vdots \\ x_M[n] \end{bmatrix} \quad n = 0, 1, \ldots, N-1, \tag{1}$$

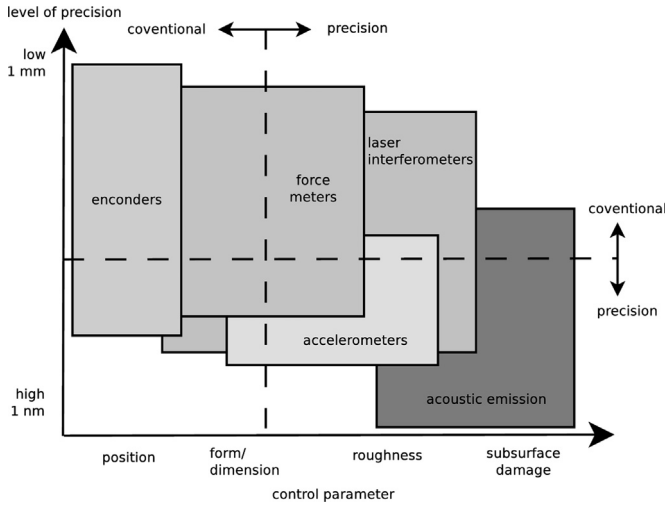

Fig. 1. Sensor sensitivity to different levels of machining precision and error control parameters. Taken from [38] and edited.

where $x_i[n]$ is the output of the ith sensor at instant n. A reasonable observation model for $x_i[n]$ is given by

$$x_i[n] = s[n] + w_i[n] \tag{2}$$

where $s[n]$ and $w_i[n]$ correspond to the signal and noise components of $x_i[n]$, respectively. Here, it is assumed that $w_i[n]$ for all i's is a sequence of random variables independent and identically distributed by some probability density function (PDF). A reasonable PDF for the noise is the WGN [42], where each random variable is uncorrelated with all the others. This leads to $w_i[n] \sim \mathcal{N}(0, \sigma_i^2)$, which denotes a Gaussian distribution with mean zero and variance σ_i^2, where σ_i^2 is the variance of the ith sensor signal. Letting $\mathbf{1} \in \mathbb{R}^M$ be a vector with all entries one, rewrite (2) as

$$\mathbf{x}[n] = \mathbf{1}^\top s[n] + \mathbf{w}[n], \tag{3}$$

where $\mathbf{w}[n]$ is an $M \times 1$ observation noise vector given by $\mathbf{w}[n] = [w_1[n] w_2[n] \ldots w_M[n]]^\top$.

The MLE approach is now utilised to provide an estimate of the signal $s[n]$, denoted by $\hat{s}[n]$, such that the conditional PDF of the noise given $s[n]$ is maximised. This MLE optimisation problem is posed as

$$\hat{s}[n] = \underset{s[n]}{\operatorname{argmax}}\, p(\mathbf{w}[n] | s[n]), \tag{4}$$

where $p(\mathbf{w}[n]|s[n])$ is the conditional PDF of the noise given $s[n]$, also known as the likelihood function. By noting (3) it is easy to see that $\mathbf{w}[n] = \mathbf{x}[n] - \mathbf{1}^\top s[n]$, then the likelihood function is

$$\begin{aligned} p(\mathbf{w}[n]|s[n]) &= p(w_1[n], w_2[n], \ldots, w_M[n]|s[n]) \\ &= p(w_1[n]|s[n]) \times p(w_2[n]|s[n]) \times \ldots \times p(w_M[n]|s[n]) \\ &= \prod_{i=1}^{M} \frac{1}{2\pi\sigma_i^2} \exp\left\{ -\frac{1}{2\sigma_i^2} (x_i[n] - s[n])^2 \right\}. \end{aligned} \tag{5}$$

To maximise the likelihood function it is easier to take the log of the expression since $s[n]$ is inside an exponent. This is known as the log-likelihood function and is given by

$$\log p(\mathbf{w}[n]|s[n]) = \sum_{i=1}^{M} \left[\log\left(\frac{1}{2\pi\sigma_i^2} \right) - \frac{(x_i[n] - s[n])^2}{2\sigma_i^2} \right]. \tag{6}$$

The next step is to take the derivative of the log-likelihood function, which gives

$$\frac{\partial}{\partial s} \log p(\mathbf{w}[n]|s[n]) = \sum_{i=1}^{M} \frac{1}{\sigma_i^2} [x_i[n] - s[n]]. \tag{7}$$

Then, by setting (7) equal to zero we can determine the value of $\hat{s}[n]$ that maximises the likelihood function leading to

$$\hat{s}[n] = \left(\sum_{i=1}^{M} \frac{1}{\sigma_i^2} \right)^{-1} \sum_{i=1}^{M} \frac{1}{\sigma_i^2} x_i[n]. \tag{8}$$

To prove that (8) is a maximum, we can check the sign of the second derivative as follows:

$$\frac{\partial^2}{\partial^2 s} \log p(\mathbf{w}[n]|s[n]) = \sum_{i=1}^{M} -\frac{1}{\sigma_i^2} < 0, \tag{9}$$

and since the term σ_i^2 is always positive, it is easy to see that the expression tends to be always negative. Hence, it is shown that the signal estimate in (8) is indeed an MLE estimate. Notably, the estimate provided by (8) will better resemble the ith sensor signal, $x_i[n]$, that yields the lowest variance among the sensor's signal.

3.2. Periodicity strength measure

The noise-corrupted signal captured by the AE sensor can be decomposed into signal and noise components as shown in (2). The signal component is a k-periodic waveform that corresponds to the cutting tool rotation, where k is the cutting tool rotation period. The noise component is aperiodic since its PDF is WGN. To determine the strength of the periodic component in a N-point discrete-time signal $\{x[0], x[1], \ldots, x[N-1]\}$, the auto-correlation coefficient is given by

$$C[k] = \frac{1}{(N-k)\sigma_x^2} \sum_{n=0}^{N-k-1} (x[n]-\mu_x)(x[n+k]-\mu_x), \tag{10}$$

where the terms μ_x and σ_x^2 denote the mean and the variance of the signal $x[n]$, respectively. The auto-correlation coefficient provides a scale-free measure of the similarity between samples as a function of the lag k. Given this, the coefficient is able to measure the system stability, such that

(i) When the system is stable or when the periodic component is dominant, the auto-correlation coefficient tends to 1.
(ii) When the system is unstable or when the aperiodic component is dominant, the auto-correlation coefficient tends to 0.

Thus, the auto-correlation coefficient is able to provide an indication of the periodic component strength, which in this case corresponds to the cutting tool rotation period. This allows us to evaluate the quality of a signal measurement during a CNC machining cutting operation that involves rotary tools.

The two approaches described above are utilised by the multi-sensor data fusion framework which is presented in the following section.

4. Multi-sensor data fusion framework

Multi-sensor data fusion [43] is composed of techniques and tools that are used for combining sensor data, or any other data that is derived from the sensory measurements, into a common representation format. The aim of multi-sensor data fusion is to improve the quality and accuracy of the collected information such that the final representation is better than, or at least not worse than, any data source collected by an individual sensor.

The multi-sensor data fusion framework proposed here aims to (i) identify which of the sensors provides the best signal representation and best location for monitoring the cutting operation, and (ii) derive a signal estimate by combining the sensory information from individual AE sensors with enhanced signal characteristics associated with the cutting operation. To achieve this aim, the steps of the framework are as follows:

1. *Signal extraction*: Collect from each sensor a discrete-time signal comprised of N observations, during a CNC machining cutting operation. It is assumed that the signals from the different sensors are in-phase.[1]
2. *Digital filtering*: Filter the ith sensor signal by applying a digital filtering technique and let it be denoted by x_i. It is recommended to use a band-pass filter with an upper and lower cutoff frequency higher and lower, respectively, than the theoretical tool cutting frequency. Let f_{up} and f_{down} denote the upper and lower cutoff frequency, respectively.
3. *Signal normalisation*: Given that the AE sensors have been positioned at different locations within the CNC machine, different levels of signal attenuation are expected between them. To account for the disparate levels of signal attenuation, each sensor signal level is normalised as follows:
   (i) let the amplitude of the jth peak in the ith sensor signal be denoted by p_j then determine the median of the amplitude of the first 20 peaks as
   $$R_i = \text{median}(\{p_1, p_2, \ldots, p_{20}\}); \tag{11}$$
   (ii) determine a normalisation factor for the ith sensor as
   $$a_i = \min_{j=1,\ldots,M}(R_j)/R_i; \tag{12}$$
   (iii) let the normalised ith sensor signal be given by
   $$y_i[n] = a_i x_i[n] \quad n = 0, 1, \ldots, N-1. \tag{13}$$

[1] Since a set of discrete-time signals are collected, these need to be in-phase to ensure that the waveforms in the generated signal do not cancel out. This issue has been handled directly by the multi-channel sound card used in this study.

4. *Sensor preference-weight*: Let the auto-correlation coefficient (10) of y_i be given by C_i. The preference-weight towards the ith sensor signal is

$$W_i = \frac{C_i}{\sum_{i=1}^{M} C_i}, \quad \text{where } \sum_{i=1}^{M} W_i = 1. \tag{14}$$

Notably, for two sensors denoted by a and b, the preference-weight indicates that (i) if $W_a > W_b$ then sensor a is preferred over sensor b; (ii) if $W_a < W_b$ then sensor b is preferred over sensor a, and; (iii) if $W_a = W_b$ (or $W_a \approx W_b$) then sensors a and b are equally important.

5. *Framework output*:

(I) *Sensor selection*: Select the sensor with the highest preference-weight and let it be denoted by

$$\mathcal{S} = \arg \max_{1 \le i \le M} (W_i). \tag{15}$$

(II) *Signal estimate*: A signal estimate is determined by combining the MLE estimate in (8) with the sensor's preference-weight (14) as given by

$$\hat{s}[n] = \left(\sum_{i=1}^{M} \frac{W_i}{\sigma_i^2} \right)^{-1} \sum_{i=1}^{M} \frac{W_i}{\sigma_i^2} y_i[n], \quad n = 0, 1, \ldots, N-1, \tag{16}$$

where σ_i^2 is the variance of the signal y_i. The signal estimate in (16) favours the sensor signals with the highest preference-weight and the sensor signals with the lowest variance. The latter is true when the two signals have the same (or approximately the same) preference-weight. For instance, if the signals of sensors a and b have differing preference-weights, then (i) $\hat{s} \approx y_a$ if $W_a > W_b$ and (ii) $\hat{s} \approx y_b$ if $W_a < W_b$. Otherwise, if the two are equally important, i.e. $W_a = W_b$ (or $W_a \approx W_b$), then (a) $\hat{s} \approx y_a$ if $\sigma_a^2 < \sigma_b^2$; and (b) $\hat{s} \approx y_b$ if $\sigma_a^2 > \sigma_b^2$.

The above procedure is summarised in Framework 1. Depending on the application the user can specify: (i) the number of signal samples, (ii) the number of sensors, and (iii) the upper and lower cutoff frequencies for digital filtering. The above framework is limited to periodic transient signals generated by the interaction between the cutting tool and the workpiece, such as CNC machines with rotary cutters. We now demonstrate this framework by analysis of experimental data.

Framework 1. Multi-sensor data fusion framework for CNC machining monitoring.

Input
N: Number of samples selected for analysis.
M: Number of sensors.
f_{up}: Upper cutoff frequency for digital filtering.
f_{down}: Lower cutoff frequency for digital filtering.

begin
- **Signal extraction**: Collect from each sensor a discrete−time signal comprised of N observations during a CNC machining cutting operation. The signals collected have to correspond to the same event and need to be in−phase.
- **Digital filtering**: apply a band−pass digital filtering technique with upper and lower cutoff frequency denoted by f_{up} and f_{down}, respectively.
- **Signal normalisation**: determine a normalisation factor (Equation 12) based on the median amplitude of the signal first 20 peaks (Equation 11) and use it to normalise each sensor signal as given by Equation 13.
- **Sensor preference−weight**: determine a sensor preference − weight (Equation 14) based on the auto − correlation coefficient (Equation 10).
- **Framework Output**:
- I: **Sensor selection**: select the sensor with the highest preference − weight by using Equation 15.
- II: **Signal estimate**: determine the signal estimate by combining the MLE estimate (Equation 8) with the sensor's preference − weight (Equation 14) as given by Equation 16.

end

5. Experimental results on CNC machining data

5.1. Experimental setup

Throughout the tests, the CNC milling machine used is a Bridgeport VMC 610XP[2]. This is a 3-axis high speed machining centre capable of spindle speeds up to 8000 rpm and a maximum spindle motor power of 13 kW. The workpiece material is aluminium alloy 6061-0 and the tool used for cutting is a two flute high speed steel 14 mm slot drill. The selected material was chosen because it is considered to be one of the most widely used alloys in the 6000 series and also due to its good

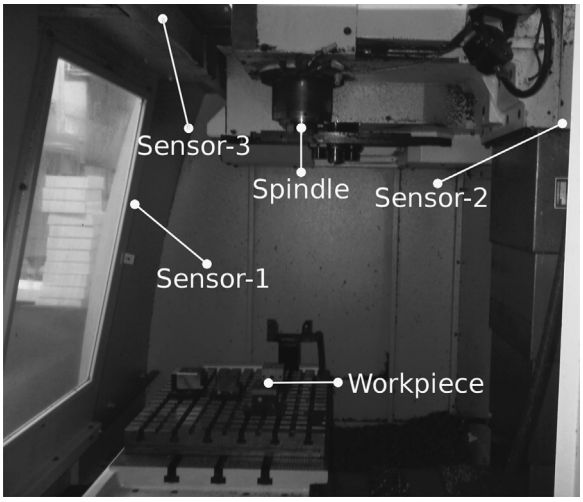

Fig. 2. Position of the AE sensors, spindle and workpiece, inside the CNC milling machine.

workability properties.[2] The same water based cutting fluid (V-Cut SS semi-synthetic) was delivered through the tool, for all the tests.

The acoustic emissions were measured by three[3] omnidirectional condenser microphones (Behringer ECM8000) with a signal bandwidth ranging from 20 Hz to 22 kHz and a sensitivity of 8.06 mV/Pa. Omnidirectional microphones, as opposed to directional microphones, have been selected to avoid having to consider directionalization techniques [13] which could further complicate the installation of the microphones inside the workspace enclosure. The frequency response of the microphone is shown in Fig. 3. The microphones were connected to a multi-channel sound card (Edirol UA-101) with measurements logged at 44.1 kHz. The Nyquist–Shannon sampling theorem [44] asserts that for a complete representation of the signal the bandwidth needs to be less than half of the sampling rate. This is the case for this setup since the bandwidth (22 kHz–20 Hz = 21,980 Hz) is less than half of the sampling rate (44.1 kHz/2 = 22,050 Hz), i.e., 21,980 Hz $<$ 22,050 Hz.

The position of the AE sensors inside the CNC milling machine is shown in Fig. 2. Note that the AE sensors have been positioned around the workpiece but have not been attached to the cutting tool or workpiece, which is a common trend throughout the literature. The justification for this lies in the fact that there is a water based cutting fluid being delivered through the tool and also that there is a significant amount of vibration close to the cutting area due to the contact between workpiece and the cutting tool. Hence, to reduce the contamination of the measured signal by those two noise sources it has been decided to position the AE sensors at a safe distance away from the workpiece centre. The cables that connect the AE sensors to the multi-channel sound card were then fixed to the walls of the CNC milling machine interior using adhesive tape to prevent the AE sensors from moving during the cutting operation. The three chosen locations were selected apart from each other deliberately by taking into account the safety of the microphones from the water based cutting fluid and also from the vibration of the structure. As a result, the chosen locations meant that the distance between each sensor and the workpiece centre is 63 cm for Sensor-1, 105 cm for Sensor-2, and 119 cm for Sensor-3. During the cutting operation tests, it is expected that the amplitude of the measured AE signal to change when measured from a fixed position since the spindle (with a cutting tool attached) moves 23 cm horizontally along the workpiece whilst cutting a slot. Hence, for consistency and to reduce the Doppler effect,[4] all the AE signals that have been considered for analysis have been extracted when the spindle is in the centre of the workpiece. As an example, it is shown on Fig. 4 (top) all the measured AE signals during the complete cutting operation, and on Fig. 4 (bottom) it is shown the selected segment that corresponds to a time frame of 0.3 s (the exact number of points is $N = 13{,}232$). In subsequent plots the signal waveform represented is many times truncated to the first 0.1 s, or to lower time frames, in order to improve the signal visualisation.

To reduce any source of noise that might affect the signal information, a band-pass second-order Butterworth filter [45] is utilised, with parameters

(i) a lower cutoff frequency (f_{down}) equal to 20 Hz which corresponds to the microphone lowest bandwidth frequency; and
(ii) an upper cutoff frequency (f_{up}) equal to 1000 Hz since the microphone frequency response in the range]1000; 22,000] (Hz) is characterised by high oscillations as reported in Fig. 3.

[2] Although different types of materials might have an influence on the generated acoustic emissions, it is not within the scope of this work to study these effects.

[3] The given framework does not have an upper limit on the number of microphones that can be used, however, for safety reasons it was decided that a maximum of three microphones could be placed inside the CNC machine during the cutting operation.

[4] Given that the distance between the spindle and each sensor changes during the cutting process (caused by the spindle movement), it is expected that the captured signal would change as well. The Doppler effect in this situation can lead to change in frequency of the signal which affects the reliability of the framework since the periodic component strength of the signal would change as well.

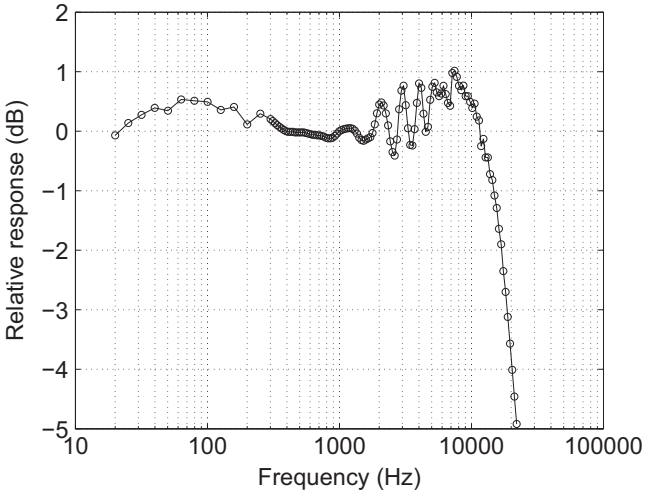

Fig. 3. Frequency response for microphone Behringer ECM8000. The calibration data has been provided by Behringer upon request.

5.2. Acoustic transient signals

The cutting tool in milling operations is utilised to remove material from the workpiece by shear deformation. This is accomplished by the movement of the teeth, present in the tool, which hit the workpiece and the vibration of the impact produces the acoustic emission. For one particular set of cutting parameters the waveform of the acoustic emission captured by Sensor-1 is represented in Fig. 5(a). For this particular dataset it is expected for the tool to conduct approximately 2.4 rotations which leads to four transient signals since there are two teeth on the tool. This is by knowing that the spindle speed has been set to 1700 rpm and that the selected time frame corresponds to 0.085 s. The same signal is also represented in the frequency domain in Fig. 5(b), where the frequency of the tool teeth hitting the workpiece, denoted here by tooth-impact frequency, is represented by the highest peak. The other lower peaks that are integer multiples of the tooth-impact frequency are known as harmonics. The tooth-impact frequency is given by

$$f_{tool} = n \times \frac{m}{60}, \tag{17}$$

where n is the number of teeth on the tool, m is the spindle speed in rpm and the tooth-impact frequency is given in cycles per second, or Hz. For a spindle speed of 1700 rpm the tooth-impact frequency is approximately 56.7 Hz and this frequency is shown in Fig. 5(b) by a dotted vertical line. The waveform in Fig. 5(a) is not purely sinusoidal and this means that the energy released by the cutting forces is not totally concentrated on the tooth-impact frequency, and as a result, some energy gets distributed along the frequency spectrum. In particular, the frequency components that are integer multiples of the tooth-impact frequency, also known as harmonics, are boosted since they are easier to excite and therefore they can be easily identified in the frequency spectrum as shown in Fig. 5(b).

The signal in Fig. 5(a) along with the corresponding frequency spectrum (Fig. 5(b)) provides the machinist (or operator) the information that the cutting tool is hitting the workpiece at a rate that corresponds to the tooth-impact frequency for the given spindle speed. That is, for a spindle speed of 1700 rpm the measured highest frequency peak corresponds to the tooth-impact frequency of 56.7 Hz and any other peaks in the frequency spectrum are the harmonics of the tooth-impact frequency.

In the given application the framework operates in the frequency range 20–1000 Hz and the acoustic transient signal generated in that range is then used to monitor the cutting operation. This implies that a good SNR for AE in this case depends on other events (or simply noise) that might exist in the same frequency range. The event of interest in this application is the interaction between cutting tool and workpiece that is defined by the spindle speed, set here between 1700 and 4000 rpm.

5.3. Demonstration of Framework 1 on a single set of machining parameters

This section demonstrates the working of Framework 1 when applied to a single set of sensor measurements, corresponding to one set of machining parameters. The parameters are 4000 rpm spindle speed, 1800 mm/min feed rate, and 2 mm depth of cut. These parameters have been selected because the captured signals by the AE sensors present disparate levels among their periodic component strength. The application of the framework steps is as follows:

1. *Signal extraction*: For the above set of parameters the signal waveform obtained by Sensor-1, Sensor-2 and Sensor-3 is represented in Fig. 6(a), (b), and (c), respectively. In the three cases it is difficult to visualise the signal waveform since the

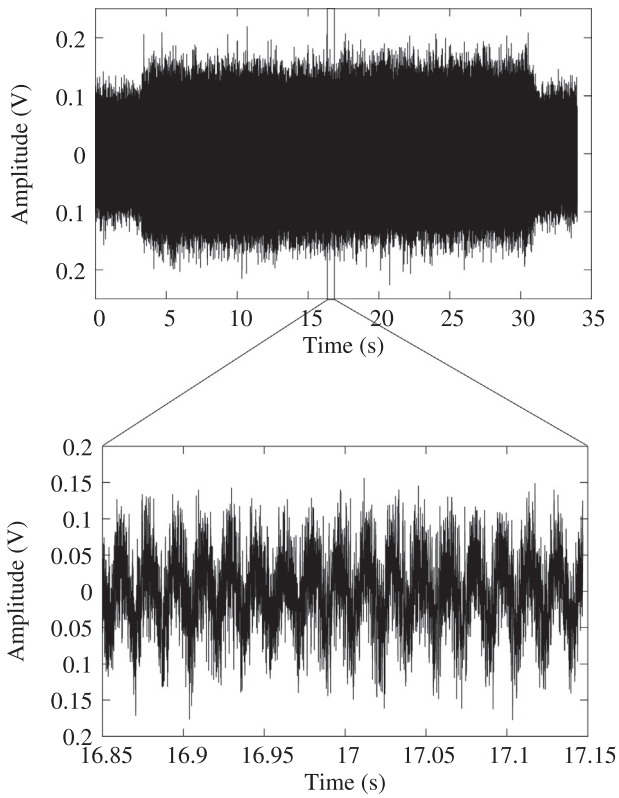

Fig. 4. AE signal captured during a complete cutting operation is shown on top and the selected segment is shown on the bottom. Note that the signal segment selected corresponds to the time instant when the spindle is in the centre of the workpiece.

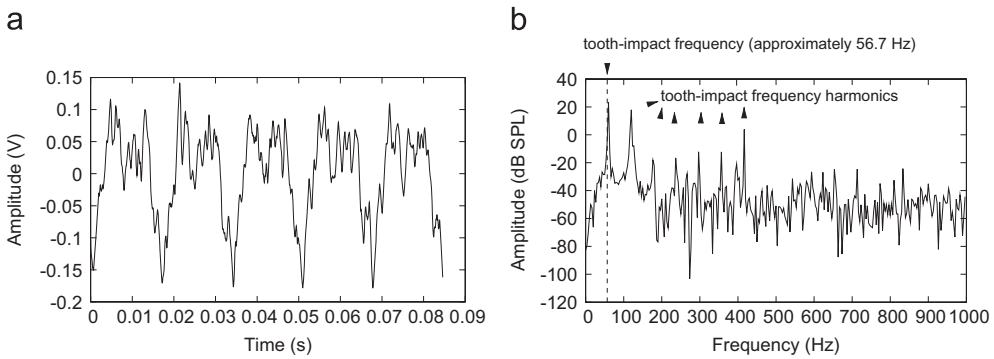

Fig. 5. Acoustic transient signals captured during a milling operation. The signal as been captured by Sensor-1 and the cutting parameters are 1700 rpm spindle speed, 510 mm/min feed rate, and 4 mm depth of cut. The signal has been filtered by a band-pass filter as detailed in Section 5.1. The vertical dotted line in (b) denotes the tooth-impact frequency. (a) Waveform and (b) frequency spectrum.

SNR is low. Also, note that the amplitude of the signal changes with the sensor proximity to the workpiece. In that, Sensor-1 is the closest to the cutting operation while the farthest sensor is Sensor-3.

2. *Digital filtering*: The application of the Butterworth band-pass filter with $f_{down} = 20$ Hz and $f_{up} = 1000$ Hz improves the SNR and unveils the signal waveform as evident in Fig. 6(d), (e), and (f), for Sensor-1, Sensor-2 and Sensor-3, respectively. For the represented time frame of 0.1 s, it is expected for the tool to execute approximately 6.7 rotations given that the spindle speed has been set to 4000 rpm. As a result, it is expected for the tool teeth to hit the workpiece at least 13 times and the same number of transient signals have to be represented in the signal waveform captured by the sensors. The 13 transient signals can be visualised in Sensor-1 waveform while the quality deteriorates as we move to Sensor-2 and to Sensor-3. This indicates that Sensor-1 provides a signal with the highest periodic component strength when compared with the other sensors.

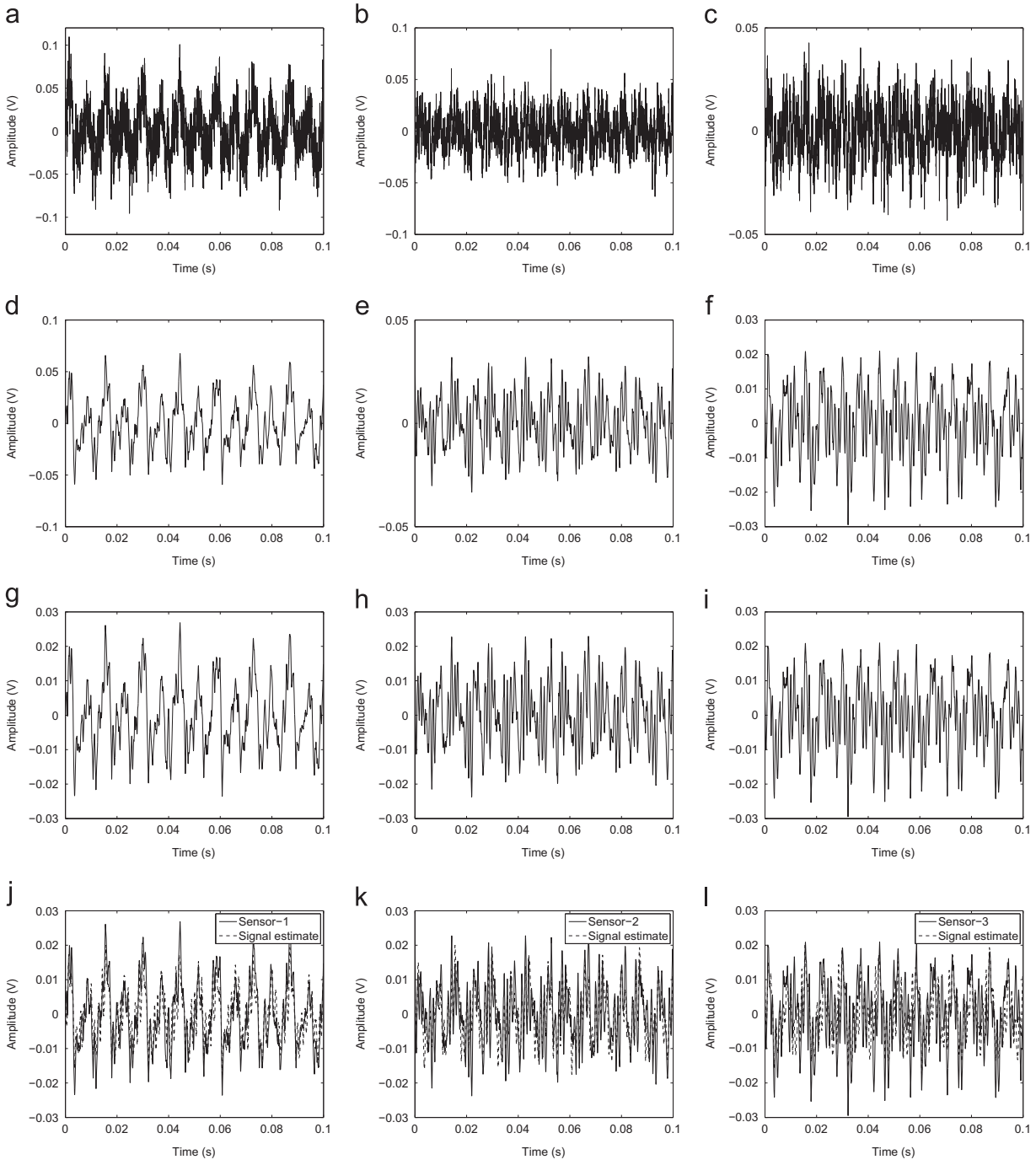

Fig. 6. Demonstration of Framework 1 on a single set of machining parameters. The plots shows the signal waveform obtained along the framework steps. The cutting parameters are 4000 rpm spindle speed, 1800 mm/min feed rate, and 2 mm depth of cut. (a) Sensor-1: signal extraction. (b) Sensor-2: signal extraction. (c) Sensor-3: signal extraction. (d) Sensor-1: digital filtering. (e) Sensor-2: digital filtering. (f) Sensor-3: digital filtering. (g) Sensor-1: signal normalisation. (h) Sensor-2: signal normalisation. (i) Sensor-3: signal normalisation. (j) Sensor-1: signal estimate. (k) Sensor-2: signal estimate. (l) Sensor-3: signal estimate.

3. *Signal normalisation*: For each sensor signal the average peak amplitude and the corresponding normalisation factor obtained are
   (a) $R_1 = 0.0431$ and $a_1 = 0.0171/0.0431 = 0.3975$;
   (b) $R_2 = 0.0240$ and $a_2 = 0.0171/0.0240 = 0.7120$;
   (c) $R_3 = 0.0171$ and $a_3 = 0.0171/0.0171 = 1.0000$.

This leads to the normalised waveforms as shown in Fig. 6(g), (h), and (i), for Sensor-1, Sensor-2 and Sensor-3, respectively. Sensor-3 yields the lowest peak amplitude among the sensors and therefore it is used as a reference for normalising the other sensors signals while its amplitude remains unchanged. Whereas the lowest factor is attributed to Sensor-1 since its peak amplitude is the highest among the sensors.

4. *Sensor preference-weight*: For each sensor the periodicity strength measure and the corresponding preference-weight obtained are
   (a) $C_1=0.7035$ and $W_1=0.4575$;
   (b) $C_2=0.4516$ and $W_2=0.2937$;
   (c) $C_3=0.3827$ and $W_3=0.2489$.

5. *Framework output*:
   (I) *Sensor selection*: Sensor-1 yields the highest periodic component strength while the lowest one is attributed to Sensor-3. This implies that the selected sensor for the given cutting parameters is Sensor-1, that is, $\mathcal{S}=1$. To analyse this, consider the frequency spectrum shown for the three sensor signals in Fig. 7. Note that the tooth-impact frequency peak in Sensor-1 (Fig. 7(a)) is comparatively higher than the corresponding harmonics when compared with the same peak in Sensor-2 (Fig. 7(b)) and Sensor-3 (Fig. 7(c)). This explains why it is possible to better identify the transient signals generated by the cutting operation which are represented in the waveform for Sensor-1 (Fig. 6(g)) than that shown for both Sensor-2 (Fig. 6 (h)) and Sensor-3 (Fig. 6(i)). This validates the identification of Sensor-1 as the selected sensor since it is shown to capture better the cutting operation when compared with the other sensors. Moreover, Sensor-3 reports the tooth-impact frequency with the lowest amplitude which makes the signal waveform more susceptible to be affected by the harmonics and any other sources of noise. This explains why Sensor-3 reports the lowest periodic component strength among the sensors. Consequently, the preference-weights reported above reflects the relative strength of the periodic component among sensors and by decreasing order of magnitudes it gives $W_1 > W_2 > W_3$.
   (II) *Signal estimate*: The obtained signal estimate is shown against the signal of each individual sensor in Fig. 6(j), (k) and (l), for Sensor-1, Sensor-2 and Sensor-3, respectively. Notably, the signal estimate resembles better that obtained by Sensor-1 when compared with Sensor-2 and Sensor-3. This is expected since the preference-weight attributed to Sensor-1 is the highest among the sensors. The signal estimate waveform is represented on its own in Fig. 8(a) and the corresponding frequency spectrum in Fig. 8(b). Note that the transient signals that characterise the tooth-impact frequency are all perceptible in Fig. 8(a) while in Fig. 8(b) the highest peak corresponds to the tooth-impact frequency. The strength of the periodic component of the signal estimate as measured by the periodic strength measure (Eq. (10)) is equal to 0.8217 which is considered to be an improvement over the individual sensors given above.

Remarkably, for the selected set of cutting parameters, if only one AE sensor is available and its position is the same as Sensor-2 or Sensor-3, it would not be possible to monitor the machining cutting process with precision. Hence, endowing a

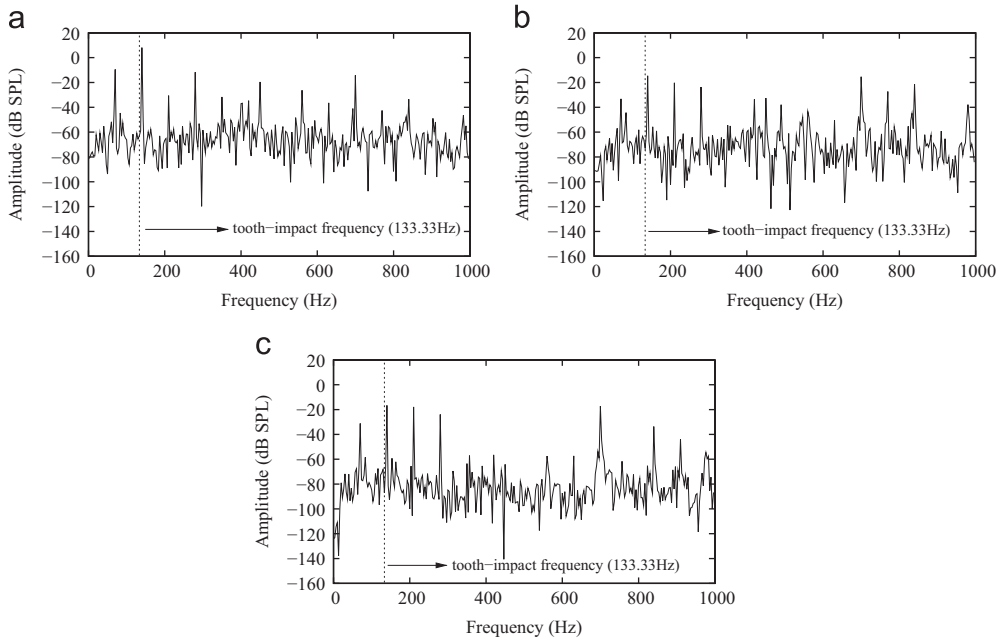

Fig. 7. Frequency spectrum for Sensor-1 (a), Sensor-2 (b), and Sensor-3 (c). The cutting parameters are 4000 rpm spindle speed, 1800 mm/min feed rate, and 2 mm depth of cut. The vertical dashed line indicates the theoretical tooth-impact frequency which corresponds to approximately to 133.33 Hz.

monitoring system with a multi-sensor data fusion framework is clearly justified given that

(i) The effect of noise is minimised since the system relies on more than one sensor. Note that relying on Sensor-1 is clearly better than relying on either Sensor-2 or Sensor-3.
(ii) The signal interpretation is likely to improve, which leads to a more reliable and robust monitoring system. The signal characteristics that better describe the machining cutting operation, that is, the transient signals that characterise the tool-impact frequency have been transferred to the signal estimate. This is reflected in Fig. 8(a) and (b) for time and frequency domain, respectively.

5.4. Experimental results for a wider range of machining parameters

In this section a set of experimental results have been conducted for a wider range of machining parameters which include the following machining conditions: spindle speed ranging from 1700 to 4000 (rpm), feed rate ranging from 510 to 2000 (mm/min), and depth of cut ranging from 1 to 4 (mm). For these parameters, the strength of the signal periodic component (C) is reported first among the sensors in Table 1 and then between the selected sensor and the signal estimate in Table 2. To facilitate the analysis, the best results reported in the tables have been highlighted in bold. Now considering Table 1, note that the strength of the signal periodic component is influenced by the spindle speed and the selected sensor corresponds to

(i) Sensor-1: for all cases corresponding to 4000 rpm and for the majority of cases corresponding to 2850 rpm.
(ii) Sensor-2: for all cases corresponding to 2275 rpm and 3425 rpm, and for some cases corresponding to 2850 rpm.
(iii) Sensor-3: for the majority of cases corresponding to 1700 rpm.

The above observations indicate that the strength of the signal periodic component is highly influenced by the position of the sensors and by the spindle speed. This further suggests that the AE sensors are sensitive to other sources of noise that could occur inside the CNC machine at different locations and that these sources of noise change depending on the selected cutting parameters. This would mean that determining the ideal position of a single sensor that would maximise the strength of the periodic component for a wide range of cutting parameters might be difficult due to the following reasons:

1. The position of a single AE-sensor that is commonly adopted throughout the literature is as close as possible to the machining zone to ensure minimum damping. However, this is not always possible due to other events that might occur in the proximity of the machining zone, such as water based cutting fluid being delivered through the tool, and vibration close to the cutting area due to contact between workpiece and cutting tool. This meant that for the given CNC machine and cutting operation the closest safest position to the workpiece centre was 63 cm, which corresponds to Sensor-1.
2. The results in Table 1 have revealed that the best sensor location is highly influenced by the selected spindle speed. Hence, attempting to select one single position for all tests might be ideal for a given spindle speed but it is not ideal for a wide range of cutting parameters.

Consider now Table 2 where a comparison is conducted between the signal estimate provided by Framework 1 and the best values reported by the sensors. The periodic component strength reported by the signal estimate is higher than any sensor signal in 52 out of 100 cases. In the remaining cases the performance of the signal estimate is very close to the

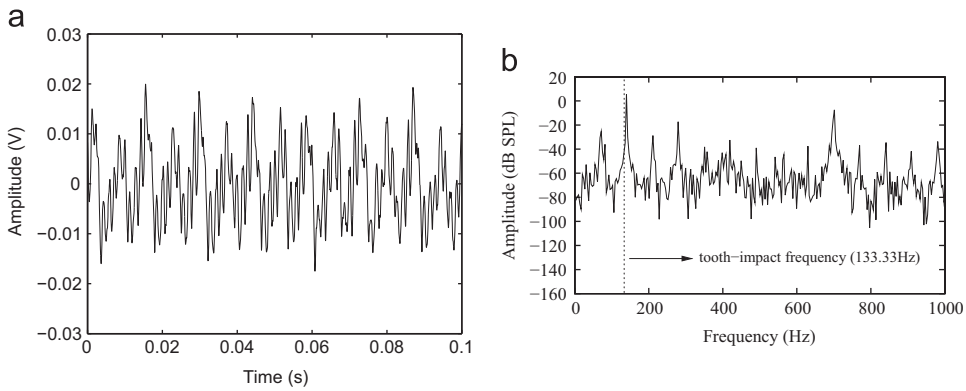

Fig. 8. Time (a) and frequency (b) domains for signal estimate. The cutting parameters are 4000 rpm spindle speed, 1800 mm/min feed rate, and 2 mm depth of cut. In (b) the vertical dashed line indicates the theoretical tooth-impact frequency which corresponds to approximately to 133.33 Hz.

Table 1
Periodicity strength measure (C): comparative analysis between the sensor signals for a wide range of machining parameters. The values in bold correspond to the selected sensor (S).

Feed rate (mm/min)	Depth of cut (mm)											
	Sensor-1				Sensor-2				Sensor-3			
	1	2	3	4	1	2	3	4	1	2	3	4
Spindle speed: 1700 rpm												
510	0.5963	0.8408	0.8391	0.9438	0.6960	0.8678	0.8924	**0.9796**	**0.7549**	**0.8963**	**0.9257**	0.9714
595	0.5675	0.8212	0.7798	0.9433	**0.6949**	0.8786	**0.9321**	0.9826	0.6640	**0.9147**	0.9035	**0.9749**
680	0.6525	0.8184	0.9000	0.9336	0.6746	0.8811	**0.9605**	**0.9768**	**0.7236**	**0.9104**	0.9575	0.9627
765	0.6503	0.8162	0.8935	0.9380	0.7332	0.8545	**0.9582**	**0.9757**	**0.7467**	**0.9025**	0.9550	0.9582
850	0.6691	0.7966	0.8887	0.9391	0.7341	0.8681	0.9478	**0.9530**	**0.7482**	**0.9030**	**0.9483**	0.9213
Spindle speed: 2275 rpm												
682	0.6694	0.8070	0.8591	0.8784	**0.7693**	**0.9446**	**0.9712**	**0.9703**	0.4927	0.8458	0.9248	0.9508
796	0.7091	0.8130	0.8502	0.8610	**0.7350**	**0.9517**	**0.9751**	**0.9398**	0.4473	0.8962	0.9496	0.9181
910	0.6805	0.8803	0.8738	0.8795	**0.7784**	**0.9661**	**0.9613**	**0.9251**	0.4485	0.9458	0.9294	0.9056
1024	0.7350	0.8439	0.9128	0.8647	**0.8337**	**0.9714**	**0.9854**	**0.9275**	0.6521	0.9674	0.9842	0.9163
1137	0.7374	0.8004	0.9115	0.7100	**0.8806**	**0.9656**	**0.9833**	**0.8954**	0.7172	0.9637	0.9785	0.8825
Spindle speed: 2850 rpm												
855	0.9151	0.9619	**0.9769**	**0.9785**	**0.9214**	**0.9679**	0.9549	0.9533	0.7371	0.8946	0.9472	0.9391
997	0.9270	**0.9708**	**0.9741**	0.9727	**0.9383**	0.9700	0.9460	**0.9733**	0.7523	0.8417	0.9467	0.9544
1140	**0.9552**	**0.9719**	**0.9652**	0.9595	0.9450	0.9643	0.8728	**0.9702**	0.7421	0.8480	0.8734	0.9497
1282	**0.9498**	**0.9688**	**0.9809**	0.9380	0.9458	0.9383	0.9623	**0.9715**	0.7554	0.8471	0.9444	0.8712
1425	**0.9548**	**0.9699**	0.9653	0.9469	0.9508	0.9264	**0.9690**	**0.9621**	0.7367	0.8354	0.9034	0.8778
Spindle speed: 3425 rpm												
1027	0.5666	0.8837	0.9335	0.9433	**0.9105**	**0.9818**	**0.9915**	**0.9950**	0.6663	0.9242	0.9698	0.9751
1199	0.7095	0.9241	0.9159	0.9450	**0.9315**	**0.9879**	**0.9915**	**0.9944**	0.7994	0.9630	0.9613	0.9738
1370	0.7371	0.9203	0.9299	0.9407	**0.9432**	**0.9873**	**0.9928**	**0.9942**	0.8383	0.9631	0.9762	0.9690
1586	0.7567	0.9068	0.9423	0.9481	**0.9564**	**0.9828**	**0.9935**	**0.9958**	0.8488	0.9650	0.9793	0.9757
1712	0.8246	0.8955	0.9407	0.9545	**0.9670**	**0.9832**	**0.9929**	**0.9947**	0.8992	0.9628	0.9800	0.9749
Spindle speed: 4000 rpm												
1200	**0.4972**	**0.5869**	**0.7885**	**0.8475**	0.1892	0.3097	0.4468	0.6844	0.3900	0.2330	0.5104	0.7679
1400	**0.6307**	**0.5620**	**0.8223**	**0.8245**	0.2097	0.2678	0.5330	0.7515	0.4094	0.2620	0.5638	0.6895
1600	**0.6029**	**0.5810**	**0.8633**	**0.8585**	0.1554	0.1866	0.6269	0.7604	0.3780	0.2322	0.7109	0.6429
1800	**0.5473**	**0.7035**	**0.8585**	**0.8281**	0.1639	0.4516	0.6253	0.7630	0.1756	0.3827	0.6750	0.5805
2000	**0.5887**	**0.7206**	**0.8628**	**0.8720**	0.1004	0.5714	0.6885	0.8400	0.2239	0.6158	0.7317	0.7002

best sensor values which is reflected in the absolute difference reported in Table 2. The results have also shown that when all the sensors have a strong periodic component then the periodicity strength of the signal estimate is not likely to show much improvement. This is the case for instance when the spindle is equal to 3425 rpm and the depth of cut higher than 2 mm.

One particular observation relates to the fact that the lowest periodicity component strength reported by the signal estimate corresponds to a depth of cut of 1 mm when compared with other cases. To analyse this, consider a single test where the cutting parameters are 4000 rpm spindle speed, 1800 mm/min feed rate, and 1 mm depth of cut. For this particular situation, Fig. 9 shows the time and the frequency domain of the sensors and the signal estimate. Notably, the tooth-impact frequency peak of Sensor-2 is extremely low when compared with the corresponding harmonics which is reflected in both time and frequency domains as shown in Fig. 9(b) and (e), respectively. This is likely to have a severe impact on the periodic component strength of the signal estimate despite the low preference-weight attributed to the sensor by the framework. Besides this, it is also reported for Sensor-1 and Sensor-3 that the amplitude of the tooth-impact frequency peak is relatively close to the corresponding harmonics as shown in Fig. 9(d) and (f), respectively. As a result, the amplitude of the tooth-impact frequency peak of the signal estimate as shown in Fig. 9(h) is also relatively close to at least one of the harmonics which clearly affects the periodic component strength. This suggests that when the periodic component strength of the signals involved in the ensemble is weak, it is very likely for the periodic component strength of the signal estimate to be weak as well.

The above observations have shown experimentally that the proposed multi-sensor data fusion framework is able to enhance the periodic component strength of the sensor signal when a comparison is conducted (i) with the worst performing sensor for all cutting conditions, and (ii) with the best performing sensor for the majority of the cutting conditions. To achieve this, the signal estimate derivation relies on those AE sensors with a strong periodic component. As a result, the interpretation of AE signals that have originated from CNC machining operations is likely to improve which leads

Table 2
Periodicity strength measure (C): comparative analysis between the best sensor signals and the signal estimate for a wide range of machining parameters. The entries in "selected sensor" correspond to the bold values in Table 1. The entries in "absolute difference" are determined between the values in 'selected sensor' and 'signal estimate". The best results correspond to the values in bold.

Feed rate (mm/min)	Depth of cut (mm)											
	Selected sensor				Signal estimate				Absolute difference			
	1	2	3	4	1	2	3	4	1	2	3	4
Spindle speed: 1700 rpm												
510	0.7549	0.8963	0.9257	0.9796	**0.8217**	**0.9320**	**0.9492**	**0.9822**	0.0668	0.0357	0.0235	0.0026
595	0.6949	0.9147	0.9321	**0.9826**	**0.7727**	**0.9308**	**0.9340**	0.9805	0.0778	0.0161	0.0019	0.0021
680	0.7236	0.9104	0.9605	0.9768	**0.7997**	**0.9248**	**0.9681**	**0.9781**	0.0761	0.0144	0.0076	0.0013
765	0.7467	0.9025	0.9582	0.9757	**0.8230**	**0.9206**	**0.9646**	**0.9782**	0.0763	0.0181	0.0064	0.0025
850	0.7482	0.9030	0.9483	0.9530	**0.8380**	**0.9099**	**0.9554**	**0.9632**	0.0898	0.0069	0.0071	0.0102
Spindle speed: 2275 rpm												
682	0.7693	**0.9446**	**0.9712**	**0.9703**	**0.8126**	0.9404	0.9552	0.9665	0.0433	0.0042	0.0160	0.0038
796	0.7350	0.9517	**0.9751**	0.9398	**0.8424**	**0.9526**	0.9592	**0.9560**	0.1074	0.0009	0.0159	0.0162
910	0.7784	0.9661	0.9613	0.9251	**0.7968**	**0.9709**	**0.9637**	**0.9547**	0.0184	0.0048	0.0024	0.0296
1024	0.8337	**0.9714**	**0.9854**	0.9275	**0.8820**	0.9658	0.9771	**0.9414**	0.0483	0.0056	0.0083	0.0139
1137	0.8806	**0.9656**	**0.9833**	**0.8954**	**0.9072**	0.9526	0.9767	0.8855	0.0266	0.0130	0.0066	0.0099
Spindle speed: 2850 rpm												
855	0.9214	0.9679	**0.9769**	**0.9785**	**0.9531**	**0.9839**	0.9735	0.9656	0.0317	0.0160	0.0034	0.0129
997	0.9383	**0.9708**	0.9741	0.9733	**0.9529**	0.9678	**0.9796**	**0.9858**	0.0146	0.0030	0.0055	0.0125
1140	**0.9552**	**0.9719**	**0.9652**	0.9702	0.9402	0.9659	0.9554	**0.9849**	0.0150	0.0060	0.0098	0.0147
1282	**0.9498**	**0.9688**	0.9809	0.9715	0.9383	0.9572	**0.9844**	**0.9735**	0.0115	0.0116	0.0035	0.0020
1425	**0.9548**	**0.9699**	0.9690	0.9621	0.9343	0.9652	**0.9730**	**0.9734**	0.0205	0.0047	0.0040	0.0113
Spindle speed: 3425 rpm												
1027	**0.9105**	**0.9818**	**0.9915**	**0.9950**	0.8390	0.9543	0.9795	0.9934	0.0715	0.0275	0.0120	0.0016
1199	**0.9315**	**0.9879**	**0.9915**	**0.9944**	0.9005	0.9769	0.9725	0.9927	0.0310	0.0110	0.0190	0.0017
1370	**0.9432**	**0.9873**	**0.9928**	**0.9942**	0.9020	0.9737	0.9824	0.9948	0.0412	0.0136	0.0104	0.0006
1586	**0.9564**	**0.9828**	**0.9935**	**0.9958**	0.9111	0.9759	0.9836	0.9954	0.0453	0.0069	0.0099	0.0004
1712	**0.9670**	**0.9832**	**0.9929**	**0.9947**	0.9459	0.9733	0.9843	0.9809	0.0211	0.0099	0.0086	0.0138
Spindle speed: 4000 rpm												
1200	0.4972	**0.5869**	0.7885	**0.8475**	**0.5591**	0.5692	**0.8266**	0.8309	0.0619	0.0177	0.0381	0.0166
1400	**0.6307**	0.5620	0.8223	**0.8245**	0.5648	**0.6928**	**0.8620**	0.8044	0.0659	0.1308	0.0397	0.0201
1600	**0.6029**	0.5810	0.8633	**0.8585**	0.5398	**0.6629**	**0.9129**	0.8041	0.0631	0.0819	0.0499	0.0544
1800	**0.5473**	0.7035	0.8585	0.8281	0.5165	**0.8173**	**0.9058**	**0.9066**	0.0308	0.1138	0.0474	0.0785
2000	**0.5887**	0.7206	0.8628	0.8720	0.5243	**0.8708**	**0.9003**	**0.9344**	0.0644	0.1502	0.0375	0.0624

to a more reliable and robust monitoring system. As a remark, further improvements are expected if more AE sensors are added to the monitoring system.

6. Conclusion

This paper proposed a multi-sensor data fusion framework for monitoring machining operations based on rotary cutters. The framework was able to (i) identify which of the sensors provides the best signal representation and the best location for monitoring the cutting operation; and (ii) derive a signal estimate by combining the sensory information from three AE sensors during a CNC machining cutting operation. The signal estimate is characterised by an enhanced periodic component corresponding to the tool rotation period when compared with the individual AE sensors. The performance of the proposed framework has been studied for a wide range of machining parameters and a comparison has been conducted vis-à-vis the AE sensors. The experimental results have revealed that (i) the AE sensors are indeed highly sensitive to sensor location and to cutting parameters, (ii) the periodicity strength measure could identify the sensor with the best signal representation and best location for the given set of cutting parameters, and (iii) the derived signal estimate could outperform most of the individual sensor signals for the majority of the experimental tests in terms of periodic component strength. Despite this, it has also been found that if the periodic component strength of all the signals involved in the ensemble is weak, then the signal estimate is likely to have a weak periodic component as well.

This study marks a new direction for machining monitoring systems that currently rely only on one sensor. For future work, the authors endeavour to study the effect of scaling the number of sensors in the robustness and reliability of the proposed framework. Also, it is intended to implement the framework for on-line monitoring and to adapt the concept to other type of tools and machining processes.

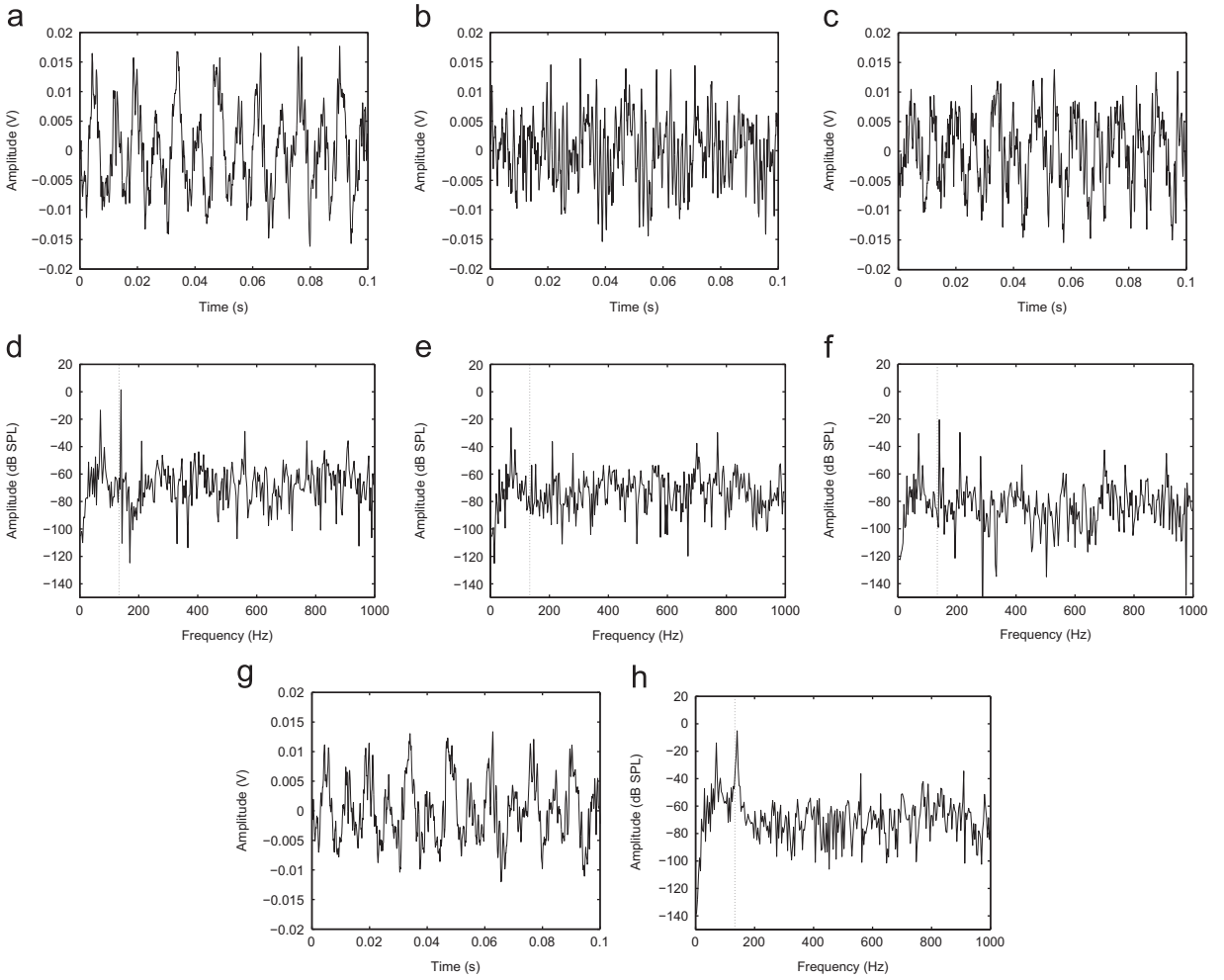

Fig. 9. Time and frequency domain for Sensor-1, Sensor-2, Sensor-3 and signal estimate. The cutting parameters are 4000 rpm spindle speed, 1800 mm/min feed rate, and 1 mm depth of cut. In the frequency domain figures the vertical dashed line indicates the theoretical tooth-impact frequency which corresponds to approximately to 133.3 Hz. (a) Sensor-1: time domain. (b) Sensor-2: time domain. (c) Sensor-3: time domain. (d) Sensor-1: frequency domain. (e) Sensor-2: frequency domain. (f) Sensor-3: frequency domain. (g) Signal estimate: time domain. (h) Signal estimate: frequency domain.

Acknowledgements

This work is partially supported by the Leverhulme Trust (Award F/00 351/AA, Formal techniques for sensor network design, management and optimisation).

References

[1] J.V. Abellan-Nebot, F.R. Subirón, A review of machining monitoring systems based on artificial intelligence process models, Int. J. Adv. Manuf. Technol. 47 (1–4) (2010) 237–257.
[2] S.Y. Liang, R.L. Hecker, R.G. Landers, Machining process monitoring and control: the state-of-the-art, J. Manuf. Sci. Eng. 126 (2) (2004) 297–310.
[3] I. Marinescu, D.A. Axinte, A critical analysis of effectiveness of acoustic emission signals to detect tool and workpiece malfunctions in milling operations, Int. J. Mach. Tools Manuf. 48 (10) (2008) 1148–1160.
[4] S. Smith, D. Dvorak, Tool path strategies for high speed milling aluminum workpieces with thin webs, Mechatronics 8 (4) (1998) 291–300.
[5] M. Monreal, C. Rodriguez, Influence of tool path strategy on the cycle time of high-speed milling, CAD Comput. Aided Des. 35 (4) (2003) 395–401.
[6] T. Chen, P. Ye, A tool path generation strategy for sculptured surfaces machining, J. Mater. Process. Technol. 127 (3) (2002) 369–373.
[7] E. Ezugwu, Key improvements in the machining of difficult-to-cut aerospace superalloys, Int. J. Mach. Tools Manuf. 45 (12–13) (2005) 1353–1367.
[8] G. Byrne, D. Dornfeld, I. Inasaki, G. Ketteler, W. König, R. Teti, Tool condition monitoring (TCM)—the status of research and industrial application, CIRP Ann.—Manuf. Technol. 44 (2) (1995) 541–567.
[9] P.R. Aguiar, P. Willett, J. Webster, Acoustic emission applied to detect workpiece burn during grinding, in: A.S. 1353, S.J. Vahaviolos (Eds.), Acoustic emission: Standards and Technology Update, American Society for Testing and Materials, West Conshohocken, PA, USA, 1999, pp. 107–124, ISBN: 0-8031-2498-8.
[10] S. Newman, A. Nassehi, R. Imani-Asrai, V. Dhokia, Energy efficient process planning for CNC machining, CIRP J. Manuf. Sci. Technol. 5 (2) (2012) 127–136.

[11] Y. Zhou, P. Orban, S. Nikumb, Sensors for intelligent machining—a research and application survey, in: IEEE International Conference on Systems, Man and Cybernetics, 1995. Intelligent Systems for the 21st Century, vol. 2, 1995, pp. 1005–1010.
[12] M.S. Lan, D. Dornfeld, Experimental studies of tool wear via acoustic emission analysis, in: Proceedings of the 10th North American Manufacturing Research Conference, McMaster University, Hamilton, Ontario, 1982, pp. 305–311.
[13] T. Delio, J. Tlusty, S. Smith, Use of audio signals for chatter detection and control, J. Eng. Ind.—Trans. Am. Soc. Mech. Eng. (ASME) 114 (2) (1992) 146–157.
[14] X. Li, A brief review: acoustic emission method for tool wear monitoring during turning, Int. J. Mach. Tools Manuf. 42 (2) (2002) 157–165.
[15] S. Mancini, G. Tumino, P. Gaudenzi, Structural health monitoring for future space vehicles, J. Intell. Mater. Syst. Struct. 17 (7) (2006) 577–585.
[16] X. Li, S. Dong, Z. Yuan, Discrete wavelet transform for tool breakage monitoring, Int. J. Mach. Tools Manuf. 39 (12) (1999) 1935–1944.
[17] L. Xiaoli, Y. Zhejun, Tool wear monitoring with wavelet packet transform-fuzzy clustering method, Wear 219 (2) (1998) 145–154.
[18] T. Blum, I. Inasaki, A study on acoustic emission from the orthogonal cutting process, ASME J. Eng. Ind. 112 (3) (1990) 203–211.
[19] S.Y. Liang, D.A. Dornfeld, Tool wear detection using time series analysis of acoustic emission, ASME J. Eng. Ind. 111 (3) (1989) 199–205.
[20] S. Kakade, L. Vijayaraghavan, R. Krishnamurthy, In-process tool wear and chip-form monitoring in face milling operation using acoustic emission, J. Mater. Process. Technol. 44 (3–4) (1994) 207–214.
[21] I. Marinescu, D. Axinte, A time–frequency acoustic emission-based monitoring technique to identify workpiece surface malfunctions in milling with multiple teeth cutting simultaneously, Int. J. Mach. Tools Manuf. 49 (1) (2009) 53–65.
[22] S. Pai, T. Nagabhushana, R. Rao, Tool condition monitoring using acoustic emission, surface roughness and growing cell structures neural network, Mach. Sci. Technol. 16 (4) (2012) 653–676.
[23] T. Reddy, C. Reddy, On-line monitoring of tool wear and surface roughness by acoustic emissions in cnc turning, Int. J. Robot. Autom. 26 (3) (2011) 305–312.
[24] S. Dey, J. Stori, A Bayesian network approach to root cause diagnosis of process variations, Int. J. Mach. Tools Manuf. 45 (1) (2005) 75–91.
[25] A. Al-Habaibeh, N. Gindy, A new approach for systematic design of condition monitoring systems for milling processes, J. Mater. Process. Technol. 107 (1–3) (2000) 243–251.
[26] Y. Niu, Y. Wong, G. Hong, An intelligent sensor system approach for reliable tool flank wear recognition, Int. J. Adv. Manuf. Technol. 14 (2) (1998) 77–84.
[27] R.E. Haber, J.E. Jiménez, C. Peres, J.R. Alique, An investigation of tool-wear monitoring in a high-speed machining process, Sensors Actuat. A: Phys. 116 (3) (2004) 539–545.
[28] R. Kuo, P. Cohen, Multi-sensor integration for on-line tool wear estimation through radial basis function networks and fuzzy neural network, Neural Netw. 12 (2) (1999) 355–370.
[29] N. Ghosh, Y. Ravi, A. Patra, S. Mukhopadhyay, S. Paul, A. Mohanty, A. Chattopadhyay, Estimation of tool wear during CNC milling using neural network-based sensor fusion, Mech. Syst. Signal Process. 21 (1) (2007) 466–479.
[30] M.J. Maeng, S.S. Cho, J.K. Chung, Tool fracture detection in end milling using cutting force and acoustic emission propagated through cutting fluid, J. Korean Soc. Precision Eng. 14 (11) (1997) 163–170.
[31] K.-N. Lou, C.-J. Lin, An intelligent sensor fusion system for tool monitoring on a machining centre, Int. J. Adv. Manuf. Technol. 13 (8) (1997) 556–565.
[32] R. Azouzi, M. Guillot, On-line prediction of surface finish and dimensional deviation in turning using neural network based sensor fusion, Int. J. Mach. Tools Manuf. 37 (9) (1997) 1201–1217.
[33] Y.M. Ertekin, Y. Kwon, T.-L.B. Tseng, Identification of common sensory features for the control of CNC milling operations under varying cutting conditions, Int. J. Mach. Tools Manuf. 43 (9) (2003) 897–904.
[34] Y. Li, L. Biao He, H. Jiang Zhu, Calibration of piezoelectric ae sensor sensitivity for longitudinal wave, in: Symposium on Piezoelectricity, Acoustic Waves and Device Applications (SPAWDA), 2010, pp. 285–289.
[35] P. Sheng, G. Chryssolouris, Investigation of acoustic sensing for laser machining processes. Part 1: Laser drilling, J. Mater. Process. Technol. 43 (2–4) (1994) 125–144.
[36] R.L. Lemaster, L. Lu, S. Jackson, The use of process monitoring techniques on a cnc wood router. Part 1. Sensor selection, Forest Prod. J. 50 (7–8) (2000) 31–38.
[37] L. Grad, J. Grum, I. Polajnar, J.M. Slabe, Feasibility study of acoustic signals for on-line monitoring in short circuit gas metal arc welding, Int. J. Mach. Tools Manuf. 44 (5) (2004) 555–561.
[38] D. Dornfeld, Y. Lee, A. Chang, Monitoring of ultraprecision machining processes, Int. J. Adv. Manuf. Technol. 21 (8) (2003) 571–578.
[39] D. Lee, I. Hwang, C. Valente, J. Oliveira, D. Dornfeld, Precision manufacturing process monitoring with acoustic emission, Int. J. Mach. Tools Manuf. 46 (2) (2006) 176–188.
[40] R.A. Fisher, On the mathematical foundations of theoretical statistics, Philos. Trans. R. Soc. Lond. Ser. A, Contain. Pap. Math. Phys. Charact. 222 (1922) 309–368.
[41] I.J. Myung, Tutorial on maximum likelihood estimation, J. Math. Psychol. 47 (1) (2003) 90–100.
[42] G. Kyriazis, Uncorrelated gaussian noise assumption in harmonic analysis with integrating digital sampling voltmeters, in: Conference on Precision Electromagnetic Measurements Digest, 2008 (CPEM 2008), 2008, pp. 602–603.
[43] H.B. Mitchell, Multi-Sensor Data Fusion, Springer, Berlin, Heidelberg, 2007.
[44] C. Shannon, Communication in the presence of noise, Proceedings of the IRE 37(1), (1949) 10–21.
[45] S. Butterworth, On the theory of filter amplifiers, Wireless Eng. 7 (1930) 536–541.